Validation of Aura Microwave Limb Sounder O_3 and CO observations in the upper troposphere and lower stratosphere

N. J. Livesey[1], M. J. Filipiak[2], L. Froidevaux[1], W. G. Read[1], A. Lambert[1], M. L. Santee[1], J. H. Jiang[1], H. C. Pumphrey[2], J. W. Waters[1], R. E. Cofield[1], D. T. Cuddy[1], W. H. Daffer[1], B. J. Drouin[1], R. A. Fuller[1], R. F. Jarnot[1], Y. B. Jiang[1] B. W. Knosp[1], Q. B. Li[1], V. S. Perun[1], M. J. Schwartz[1], W. V. Snyder[1], P. C. Stek[1], R. P. Thurstans[1], P. A. Wagner[1], M. Avery[3], E. V. Browell[3], J.-P. Cammas[4], L. E. Christensen[1], G. S. Diskin[3], R.-S. Gao[5], H.-J. Jost[6], M. Loewenstein[7], J. D. Lopez[7], P. Nedelec[4], G. B. Osterman[1], G. W. Sachse[3], C. R. Webster[1]

Short title: AURA MLS UT/LS O_3 AND CO

[1]Jet Propulsion Laboratory, California Institute of Technology

[2]University of Edinburgh

[3]NASA Langley Research Center

[4]CNRS-UMR5560, Laboratoire d'Aérologie

[5]NOAA Earth Systems Research Laboratory, Chemical Sciences Division

[6]Novawave Technologies, 900 Island Dr., Redwood City, California

[7]NASA Ames Research Center

Abstract. Global satellite observations of ozone and carbon monoxide from the Microwave Limb Sounder (MLS) on the EOS Aura spacecraft are discussed with emphasis on those observations in the 215 – 100 hPa region (the upper troposphere and lower stratosphere). The precision, resolution and accuracy of the data produced by the MLS 'version 2.2' processing algorithms are discussed and quantified. O_3 accuracy is estimated at ∼40 ppbv+5% (∼20 ppbv+20% at 215 hPa) while the CO accuracy is estimated at ∼30 ppbv+30% for pressures of 147 hPa and less. Comparisons with expectations and other observations show good agreements for the O_3 product, generally consistent with the systematic errors quoted above. In the case of CO, a persistent factor of ∼2 high bias is seen at 215 hPa. However, the morphology is shown to be realistic, consistent with raw MLS radiance data, and useful for scientific study. The MLS CO data at higher altitudes are shown to be consistent with other observations.

1. Introduction

Ozone and carbon monoxide play important and distinct roles in the upper troposphere. Upper tropospheric ozone is a potent and poorly understood greenhouse gas [*Intergovernmental Panel on Climate Change*, 2001] whose abundance, ranging from tens to a few hundred parts per billion (ppbv), is influenced by a variety of factors including the abundance of precursor HO_x and NO_x species and influx of ozone rich air from the lower stratosphere. Rapid transport of boundary layer air to the upper troposphere by deep convection has a significant affect on ozone through transport of precursor species [*Prather and Jacob*, 1997]. Carbon monoxide is a byproduct of combustion, both natural and anthropogenic, and is one of the main sinks of tropospheric OH [*Jacob*, 1999], the main atmospheric oxidant. Its relatively long ($\sim$2 month) photochemical lifetime makes it a useful tracer of atmospheric motions, particularly of the long-range transport of polluted air [e.g., *Stohl et al.*, 2002; *Liu et al.*, 2003].

The Microwave Limb Sounder (MLS) [*Waters et al.*, 2006] on the Aura spacecraft [*Schoeberl et al.*, 2006b], launched on 15 July 2004, observes thermal microwave limb emission from many molecules including O_3 and CO. This paper describes MLS O_3 and CO data in the upper troposphere and lower stratosphere (UT/LS), broadly defined here as the region from $\sim 300 - 100$ hPa. With the exception of section 3.3, all the MLS data described in this paper are those produced by version 2.2 of the data processing algorithms.

Validation of the CO observations at higher altitudes is discussed by *Pumphrey et al.* [2007]. The MLS ozone product is also described in two companion papers in this issue. *Froidevaux et al.* [2007] focus on observations in the stratosphere and mesosphere, while

Jiang et al. [2007] describe comparisons of MLS O_3 data with sonde and ground-based observations, including in the altitude region discussed in this paper.

Section 2 describes the relevant aspects of the MLS instrument and data processing strategy, gives rules on appropriate screening for the UT/LS O_3 and CO data, and quantifies their typical precision, expected accuracy and spatial resolution. Section 3 describes some 'zero order' validation of these data including comparisons with non-coincident observations. Section 4 focuses on comparisons between MLS data and various co-located aircraft based observations. Finally, section 5 summarizes all these findings, and outlines plans for further validation and future versions of the MLS products.

2. MLS UT/LS O_3 and CO observations

2.1. MLS instrument operations and data description

MLS observes thermal microwave emission from the Earth's limb in five spectral regions from 118 GHz to 2.5 THz. The O_3 and CO standard products described in this paper are taken from observations in the 230 – 250 GHz spectral range. MLS looks forward from the Aura spacecraft and scans the Earth's limb vertically from the ground to ~90 km every 24.7 s.

This paper describes MLS 'Level 2' data, which are geophysical products reported along the measurement track of the instrument. These are retrieved from calibrated MLS radiance observations ('Level 1 data') by the MLS Level 2 data processing software [*Livesey et al.*, 2006]. The MLS O_3 and CO products are reported on a fixed vertical pressure grid having 6 levels per decade change in pressure in the troposphere and stratosphere, evenly spaced in

54 $\log_{10}$ pressure starting at 1000 hPa (thinning out to 3 per decade at pressures less than 0.1 hPa).
55 These profiles are evenly spaced at 1.5° great circle angle (geodetic) along the orbit track. This
56 gives 240 Level 2 profiles per orbit at fixed latitudes, synchronized to the MLS vertical scans.

57 The MLS Level 2 products are reported in Level 2 Geophysical Product (L2GP) data
58 files. Individual files describe one MLS 'standard product' (O_3, CO, H_2O etc.) for a 24
59 hour period from midnight to midnight universal time. The L2GP files store the data in an
60 HDF-EOS version 5 'swath' format. The ozone files contain additional swaths giving the
61 estimated column ozone amount above the tropopause [*Froidevaux et al.*, 2007]. The MLS
62 Version 2.2 data quality document [*Livesey et al.*, 2007] gives more information on the format
63 and contents of the MLS data files.

64 **2.2. Proper use of MLS UT/LS O_3 and CO data**

65 In addition to describing file formats and contents, the data quality document [*Livesey*
66 *et al.*, 2007] also gives detailed instructions on the proper use of all MLS data products. The
67 pertinent information for MLS UT/LS CO and O_3 is repeated here.

68 Each MLS Level 2 data point is reported with a corresponding precision value. This
69 quantifies the impact MLS radiance noise and (particularly in regions of lower measurement
70 sensitivity) the contribution of a priori information. These issues are discussed in more detail
71 in section 2.4. As an aid to users, the precisions are set to negative values in situations where
72 the retrieved uncertainty is larger than 50% of a priori uncertainty, indicating that MLS
73 contributed little information to these data and that they should not be used in scientific study.

74 Three additional data quality metrics are provided for each MLS profile. 'Status' is

an integer bit field indicating where profiles are not to be used, or may be suspect due to instrumental and/or retrieval issues. Odd values denote profiles that should never be used. Non-zero, even values indicate situations where care may be needed, typically where the retrieval algorithm detected strong cloud signatures in some radiances and chose to discard those radiances. The impact of this on MLS data varies with species and height. Such profiles are typically suitable for scientific use, though they are usually reported with poorer precision due to the fewer number of radiances used in their retrieval. Note that this is a change from v1.5, where such profiles were to be ignored in the UT/LS. More details on the 'Status' field are given in the data quality document. The 'Quality' field gives a measure of the fit achieved to the measured MLS radiances by the retrieval (larger numbers imply better fits).

The MLS data processing algorithms simultaneously retrieve multiple ($\sim$10) MLS profiles in 15° orbit sections known colloquially as 'chunks'. The 'Convergence' diagnostic compares the fit achieved across an entire 'chunk' to that expected by the retrieval algorithms. Values in the range $1.0-1.1$ indicate excellent convergence.

MLS v2.2 CO and O_3 data in the range 215 hPa to 100 hPa should only be used when:

1. The precision value for that data point is positive
2. 'Status' for that profile is an even number (this differs from the rules for v1.5 data)
3. The 'Quality' field for that profile is greater than 1.2 (note this is stricter than the stratospheric and mesospheric thresholds of 0.4 for O_3 and 0.2 for CO.)
4. 'Convergence' is less than 1.8.

The MLS v2.2 O_3 and CO data are retrieved over the range 316 – 0.00046 hPa. As will be shown later, the v2.2 O_3 and CO data at 316 hPa are not considered useful for scientific study, and only data in the range 215 – 0.0022 hPa should be used (see *Froidevaux et al.* [2007] and *Pumphrey et al.* [2007] for discssion of upper altitude limits).

2.3. Signature of UT/LS O_3 and CO in MLS radiances

Figure 1.

Figure 1 shows typical MLS radiance observations in the 240 GHz region of the spectrum, from which the UT/LS O_3 and CO products are derived. All of the strong spectral features are due to emission from O_3 lines, with the exception of the feature at ∼234.0 GHz in the lower sideband from $O^{18}O$ emission. The CO spectral line is at ∼230.5 GHz in the lower sideband and has a ∼1 K typical amplitude in the upper troposphere. The small features in this region seen at the higher tangent altitudes (e.g., red line) are due to strong emission from mesospheric CO. The UT/LS O_3 information derives from the broad spectral contrast across the spectral region, mainly seen by three of the four 'wide' channels, namely those at ∼244.5 GHz, ∼246.8 GHz and ∼247.5 GHz upper sideband frequency.

The MLS CO and O_3 data are retrieved using an optimal estimation approach [*Rodgers*, 2000; *Livesey et al.*, 2006] from these 240 GHz radiances, along with observations of the 118 GHz O_2 line for additional pointing information. In addition to O_3 and CO, this retrieval also produces estimates for HNO_3, SO_2, temperature, geopotential height and tangent pressure (along with spectrally flat 'extinction' terms). The lower part of Figure 1 shows the average fit achieved to measured radiances. The scatter about these averages (not shown) is generally consistent with the levels of noise seen in the radiances, as would be expected and desired.

The fits in the CO region are generally within ∼0.2 K, while the broad spectral structure, away from strong stratospheric features, is generally fitted within a few tenths of a Kelvin.

Although MLS observations are unaffected by thin cirrus clouds or stratospheric aerosols, thick clouds associated with deep convection can impact the MLS radiances. Emission and scattering from thick high altitude (≤∼200 hPa) clouds enhances the MLS radiance signals, while scattering by lower altitude thick clouds suppresses radiances. Such signatures are generally spectrally flat. However, large amounts of scattering from the thickest clouds can attenuate the spectral variations in MLS radiances on which the composition measurements are based. The MLS data processing algorithms retrieve a spectrally flat 'extinction' term to compensate for scattering by moderate clouds. When the algorithms detect particularly thick clouds that may significantly affect the spectral contrast, radiances from individual 1/6 s integration periods are omitted from the retrieval (noted in the 'Status' flag).

2.4. Precision, scatter and spatial resolution

Figure 2.

Each point in the retrieved MLS profiles is accompanied by an estimated 'precision' field, taken from the diagonal elements of the solution covariance matrix [*Livesey et al.*, 2006]. This mainly reflects the contributions of radiance noise to the MLS measurements. In regions where MLS is less sensitive, the uncertainty on the a priori values used as virtual measurements begins to dominate the reported precision. Figure 2 summarizes the reported precision seen in MLS UT/LS O_3 and CO measurements on 17 September 2004 in the 30°S to 30°N region, typical of all these data (although the reported UT/LS O_3 precision in winter polar regions is ∼20–40% poorer). The root mean square average of the estimated precision

(solid lines) for O_3 in the UT/LS is $20-40$ ppbv, with $\sim 15-40$ ppbv estimated for CO. Because the relationship between MLS radiances and UT/LS O_3 and CO mixing ratios is close to linear, the precision on the retrieved mixing ratios is independent of abundance.

It is useful to compare these precision estimates to the actual scatter seen in MLS data (broken lines). In cases where atmospheric variability is expected to be low compared to the MLS precision, this scatter will be comparable to the estimated precision (typically a little less, due to the influence of smoothing on the MLS retrievals [*Froidevaux et al.*, 2006]), as is seen here for CO in the mid-stratosphere. For the UT/LS CO and O_3 observations, the scatter is generally larger than the estimated precision, implying significant atmospheric variability and/or contributions from other sources of random error than radiance noise.

Figure 3.

Figure 4.

The MLS retrieval algorithms operate in a two dimensional manner, retrieving multiple profiles along the track based on information from multiple vertical limb scans [*Livesey and Read*, 2000; *Livesey et al.*, 2006]. This approach allows for the direct modeling of the impact of gradients along the forward-looking MLS line-of-sight, and for rigorous quantification of the horizontal resolution in that direction. As with most remote sounding measurements, the resolution of the retrieved data can be describing using 'Averaging Kernels' [*Rodgers*, 2000]. The two-dimensional nature of the MLS retrieval system means that these kernels describe both vertical and horizontal resolution. Figures 3 and 4 show vertical and horizontal aspects of the averaging kernels for tropical retrievals of UT/LS O_3 and CO respectively. Orbital and seasonal variations in the averaging kernels are small, and the kernels shown are representative of all the data. The vertical resolution of UT/LS O_3, as defined by the width of the kernels, is ~ 2.5 km (essentially the same as the vertical spacing of the retrieval surfaces), while the CO

data have poorer ∼4 km vertical resolution. For example, the 215 hPa MLS CO values derive ∼35% of their information from the atmospheric state at 147 hPa. The 316 hPa CO kernel has an unusual shape, indicating that these retrievals are more sensitive to CO at 215 hPa than 316 hPa, and show anti-correlations with CO at higher altitudes.

In the along-track horizontal direction, the O_3 product has single-profile resolution (∼165 km) at pressures of 100 hPa and less, with resolution closer to ∼350 km at greater pressures. The along-track resolution of the CO observations is ∼500 – 600 km. The cross-track horizontal resolution for both products is defined by the horizontal width of the MLS field of view, which, for the 240 GHz radiometer that measures O_3 and CO, is ∼6 km.

2.5. Quantification of systematic uncertainties

2.5.1. Approach

A major component of the validation of MLS data is the quantification of the various sources of systematic uncertainty. These can arise from instrumental issues (e.g., radiometric calibration, field of view characterization), spectroscopic uncertainty, and through approximations in the retrieval formulation. This section summarizes the relevant results of a comprehensive quantification of these uncertainties, performed for all MLS products. More information on this assessment is given in Appendix A of *Read et al.* [2007].

For each identified source of systematic uncertainty, its impact on MLS measurements of radiance (or pointing where appropriate) has been quantified and modeled. These modeled impacts correspond to either 2-σ estimates of uncertainties in the relevant parameter(s), or an estimate of their maximum reasonable error(s) based on instrument knowledge and/or

design requirements. The impact of these perturbations on retrieved MLS products has been quantified for each uncertainty source by one of two methods.

In the first method, sets of modeled errors corresponding to the possible magnitude of each uncertainty have been applied to simulated MLS cloud-free radiances (based on a model atmosphere) for a whole day of MLS observations. These sets of perturbed radiances have then been run through the routine MLS data processing algorithms, and the comparison between these runs and the results of the 'unperturbed' run used to quantify the systematic uncertainty in each case. The impact of the perturbations varies from product to product and among uncertainty sources. In some cases, the perturbation leads mainly to an additive bias in the product; in others, some multiplicative bias may be introduced. In most cases, some additional scatter is also introduced into the data.

Although the term 'systematic uncertainty' is often associated with consistent biases and/or scaling errors, many sources of 'systematic' error in the MLS measurement system give rise to additional scatter. For example, an error in the O_3 spectroscopy, while being a bias on the fundamental parameter, will have an impact on the retrievals of species with weaker signals (e.g., CO) that varies according to morphology of atmospheric O_3. The extent to which such terms can be expected to average down is estimated to first order by these 'full up studies' through their separate consideration of the bias and scatter each uncertainty source introduces.

Figure 5.

The difference between the retrieved product in the unperturbed run and the original 'true' model atmosphere is taken as a measure of uncertainties due to retrieval formulation and numerics. The potential impact of some remaining (typically small) uncertainties has been quantified through analytic calculation based on simplified models of the MLS measurement

Figure 6.

system [*Read et al.*, 2007]. These calculations provide only an estimate of the possible multiplicative error introduced, with no bias or scatter quantification.

2.5.2. Results

Figures 5 and 6 summarize the results of this quantification for UTLS O_3 and CO, respectively. These show the magnitudes of expected biases, additional scatters and possible scaling uncertainties the various errors may introduce into the data, and should be interpreted as 2-σ estimates of their likely magnitude.

The contribution of clouds to systematic uncertainty applies only to regions of thick cloud, and has been quantified by adding the effects of scattering from a representative cloud field to the simulated radiances. Retrievals based on these radiances (including the cloud radiance screening approach outlined in section 2.3) have been compared to the unperturbed results. The bias and scatter shown are based on consideration of only the cloudy profiles (as defined by the known amount of cloud in the 'true' fields). In the case of UT/LS O_3, this study indicates a possible cloud-induced bias of $\sim \pm 5$ ppbv with an additional scatter of $\sim \pm 40$ ppbv at 215 hPa (less at smaller pressures). The corresponding impact on CO at 215 hPa is a bias of $\sim \pm 15$ ppbv with an additional scatter of ~ 15 ppbv, with smaller impacts at lesser pressures. Both products show much larger cloud impacts ($50-80$ ppbv) for 316 hPa data.

The retrieval formulation uncertainty (grey lines) mainly reflect the difference between the retrieval of unperturbed simulated radiances and the 'true' model atmosphere. In the case of CO, a positive bias of $\sim 30 \pm 10$ ppbv is seen at 215 hPa, thought mainly to be due to the modeling of spectrally flat 'extinction' terms. This bias is likely to directly apply also to real

MLS observations. The large bias and scatter this error source introduces into the 316 hPa O_3 data make it unlikely to be useful for scientific study.

Of the remaining uncertainty sources, those related to pointing issues (red), and MLS radiometric calibration (cyan) are the most significant, with contaminating species (blue) also being important for CO. Pointing uncertainties arise from uncertainty in the width of the O_2 lines used to determine limb tangent pressure, and in the vertical offsets between the fields-of-view of the MLS 118 and 240-GHz receivers. The main component of the uncertainties associated with radiometric calibration originate from the spectral signature introduced in calibrated MLS radiances by departures from a linear response within the signal chains. In addition, standing waves within the MLS instrument contribute significantly to the systematic uncertainty in the 316 hPa CO data (O_3 data at this altitude are less affected).

Overall, this study indicates a potential bias of up to ± 25 ppbv for O_3 at 147 and 215 hPa, with an additional scatter of $\sim \pm 50$ ppbv. For 100 hPa, the bias and scatter are $\sim \pm 50$ ppbv each. Possible multiplicative errors in UT/LS O_3 are 10% at 215 hPa and 5% at smaller pressures. In the case of CO, there are potential biases of roughly ± 40, ± 30, and ± 20 ppbv at 215, 147 and 100 hPa, respectively, with a scatter of $\sim \pm 10$ ppbv. Possible scaling errors in the UT/LS CO product are around 30%. In scientific studies the accuracy quoted for each MLS data point should be the estimated bias plus the multiplicative error times the retrieved value. These findings are summarized, along with precision and resolution information in Table 1. In some cases, the estimated accuracy quoted is based on comparisons with observations shown later in this paper, rather than on the expectations from this study.

3. 'Zero order' validation of MLS UT/LS O_3/CO

3.1. Overview and comparisons with expectations

Figure 7.

Figure 8.

Figure 7 shows zonal means of ∼80 days of MLS v2.2 O_3 and CO data (distributed roughly evenly among years and seasons). The generally expected structure is seen for O_3, with larger abundances seen in or closer to the stratosphere. However, the 316 hPa O_3 values (not recommended for scientific use) show an unexpected peak in the tropics. The CO also shows expected morphology with low stratospheric abundances and generally larger values lower in the atmosphere. However, the absolute values appear too high compared to expectations at 215 and 316 hPa (in situ observations indicate that, while abundances above 150 ppbv at these altitudes are possible, average values are more typically 50 – 100 ppbv).

Figure 8 compares these zonal means (and standard deviations) to data from the MOZAIC commercial aircraft dataset [*Marenco et al.*, 1998; *Thouret et al.*, 1998; *Nédélec et al.*, 2003; *Nedelec et al.*, 2005]. MOZAIC observations rarely extend to pressures smaller than 200 hPa. There is encouraging agreement between MLS O_3 and MOZAIC observations at 215 hPa. However, MLS CO data at these altitudes exhibit a high bias compared to MOZAIC. MLS CO data at 316 hPa also show a high bias and more latitudinal structure than is seen by MOZAIC, while the 316 hPa MLS O_3 data show very little relationship to MOZAIC and generally very unexpected behavior. In all these comparisons, the strong emphasis of mid-latitude northern hemisphere observations in the MOZAIC dataset should be borne in mind.

MLS radiance observations in the upper troposphere in the 240 GHz region are dominated by emission from O_3. The poor quality of the v2.2 MLS 316 hPa O_3 implies an inability

of the retrievals to correctly interpret the radiances measured at tangent pressures from $\sim 250-316$ hPa. This in turn implies that the 316 hPa MLS upper tropospheric CO data is unlikely to be of sufficient quality for scientific use, despite having more reasonable latitudinal variations than O_3 (though with a clear high bias). The same inference applies to the 316 hPa MLS HNO_3 observations [*Santee et al.*, 2007].

The combination of this inference with the results of the systematic error study in section 2.5 and the unusual form of the 316 hPa CO averaging kernel (see Figure 4) lead to the conclusion that version 2.2 O_3 and CO at 316 hPa are not suitable for scientific use.

Figure 9.

Figure 9 shows histograms of MLS UT/LS O_3 and CO observations from $\sim$40 days of observations. The screening by 'Quality' and 'Convergence' described in section 2.2 discards some unrealistically small (often negative) values of O_3 and CO at 215 hPa in the tropics. These poor retrievals probably reflect poorly modeled cloud signatures in the MLS radiances. The O_3 histograms clearly show the influence of stratospheric air at high and mid-latitudes. While generally good agreement is seen between MLS and MOZAIC O_3, the CO histograms show the MLS data to be generally high compared to MOZAIC, with a generally larger dynamic range of values. In the mid-latitudes around 215 hPa (where the bulk of the MOZAIC data were taken) a significant fraction of the CO observations indicate abundances larger than 150 ppbv. The MLS histogram in this region shows a somewhat similar tail, albeit with a clear bias towards higher values. The fact that a similar tail is not seen in MOZAIC data at 215 hPa in the tropics (a region where convective transport of polluted air is likely to be more frequent) may simply reflect the highly sparse nature of MOZAIC observations at these latitudes.

3.2. Validity of MLS CO morphology

The high bias in v2.2 215 hPa MLS CO data indicate that the morphology, while reasonable, needs specific validation. Quantification of the CO signature in raw MLS radiance measurements is one way to gain confidence. The 240 GHz region observed by MLS is dominated by emission from ozone, along with dry air and water vapor continua. The $\sim$1 K brightness temperature CO feature is small compared to these signatures, and can only be discerned after these other contributions are characterized and removed.

Figure 10.

Here, we repeat the analysis performed in *Filipiak et al.* [2005] (for a different time period) and extend it to consider MLS CO observations at 215 hPa. MLS v2.2 CO observations for 17 – 19 September 2004 are shown in the upper half of Figure 10. Clear enhancements in CO at 147 and 215 hPa are seen over central Africa and southern Asia (region A), and also off the west coast of central America. Our analysis considers MLS radiance observations in this period from band 9 (the CO band). The continuum contributions can be largely removed by subtracting the signal seen in a nearby window region (MLS band 33 channel 3). The remaining dependence of the band 9 signal on ozone can be estimated from the behavior of the MLS radiances in the 25°S – 25°N, 150°E – 150°W region (region B in Figure 10), where MLS reports lower abundances of CO with little significant morphology. In this region, the band 9 radiances show very good correlation with those in channel 25 of band 7, a channel sensitive to UT/LS O_3 but insensitive to CO abundances and only weakly sensitive to stratospheric ozone (correlation coefficients are generally greater than 0.85, except for channels closer to the CO line center, which are more strongly affected by mesospheric CO signatures). Accordingly, a

least-squares linear fit between each band 9 channel and band 7 channel 25 in this region can be used to deduce and subtract the band 9 ozone signature in other regions.

Figure 11.

Figure 11 compares average MLS radiance observations in regions A and B and shows that the difference between these, once the continuum and ozone signatures are removed, has a clear CO signature (departure at the low frequency end is due to O_3 signatures). A simple metric of CO abundance can be defined as the average radiance in this signature seen in channels $1-7$ and $16-21$ (channels $8-15$ are affected by strong emission from mesospheric CO, while channels $22-25$ are strongly affected by ozone). The lower half of Figure 10 shows a map of this metric at 147 and 215 hPa for comparison with the CO maps in the upper half of the same figure. The overall morphology in this metric compares well with that seen in the v2.2 MLS CO data. The fitting of the O_3 signature based on tropical radiances (region B) is not generally applicable to other latitudes due to differences introduced from changes in stratospheric ozone and the contributions of the moist and dry-air continua. This metric is therefore only applicable to tropical areas.

3.3. Comparison with MLS v1.5 data

This paper describes MLS UT/LS O_3 and CO data produced by version 2.2 of the MLS data processing algorithms. The previous version of MLS data, v1.5, has been produced for the majority of days from August 2004 to the end of February 2007, and has been used in a large number of scientific studies. Version 1.5 CO data have formed the basis of several scientific papers, including the discovery of a 'tape recorder' signal [*Schoeberl et al.*, 2006a], a study of transport paths into the stratosphere [*Fu et al.*, 2005], quantification of the influence

328 of convection on upper tropospheric composition [*Folkins et al.*, 2006], and the trapping of
329 polluted air in the upper troposphere [*Li et al.*, 2005].

330 The main difference between the v1.5 and v2.2 UT/LS O_3 and CO data is a dramatic
331 reduction of the 'spikes' seen in the v1.5 data due to the impact of thick clouds on the MLS
332 radiances. This was achieved by using an atmospheric extinction term rather than a radiance
333 baseline term to retrieve the spectrally broad signatures of clouds [*Livesey et al.*, 2006].

Figure 12.

334 Figures 12 and 13 compare 1 May 2006 v1.5 and v2.2 data for UT/LS O_3 and CO,

Figure 13.

335 respectively. O_3 shows generally good agreement between the two versions. The CO, by
336 contrast, is markedly improved in v2.2 over the earlier v1.5 product. Radiance signatures
337 of thick clouds led to very high anomalous values of CO in v1.5, many of which were not
338 identified as suspect by the retrieval algorithms. In v2.2 there are far fewer anomalous values
339 and very few clearly unrealistic values not identified as bad by the retrieval. While v1.5
340 reported very high values of CO in cases of cloud contamination, v2.2 generally reports low
341 or negative values (somewhat similar behavior is seen in the O_3 product). V2.2 CO data
342 show smaller difference between the tropics and mid-latitudes at 147 hPa than is seen in v1.5,
343 bringing the data into better agreement with models such as GEOS-CHEM [*Bey et al.*, 2001].
344 The underlying high bias in v2.2 215 hPa CO was apparent also in the v1.5 data, where it was
345 exacerbated by the anomalously large values associated with unreported cloud contamination.

346 4. Comparisons with other observations

347 The validation of Aura observations has been the focus, or partial focus, of several aircraft
348 campaigns since the Aura launch. The Polar Aura Validation Experiment (PAVE) during

January/February 2005 consisted of multiple flights of the NASA DC-8 to high latitudes over North America. Measurements from this campaign include vertical profiles of ozone above and below the aircraft from Light Detection and Ranging (LIDAR) instruments and in-situ observations of both O_3 and CO. The April/May 2006 Intercontinental Chemical Transport Experiment (INTEX-B) campaign made similar observations (among many others) from the same aircraft in the Northern Pacific (generally at lower altitudes). The Houston deployments of the Aura Validation Experiment (AVE) in October/November 2004 and January/February 2005 and the Costa-Rica AVE (CR-AVE) deployment in March 2006 provided in-situ measurements of several MLS species, including O_3 and CO from the NASA high-altitude WB-57 aircraft in the tropical upper troposphere and lower stratosphere.

Comparisons with data from other satellite sensors are also possible in the UT/LS region. *Froidevaux et al.* [2007] compares MLS v2.2 O_3 data with observations from the Stratospheric Aerosol and Gas Experiment (SAGE) instruments. Similarly, *Pumphrey et al.* [2007] compare MLS v2.2 CO data with observations from the Canadian ACE satellite.

4.1. Comparisons with airborne LIDAR O_3 data

During the PAVE and INTEX-B campaigns, the DC-8 payload included two LIDAR instruments measuring ozone. The Differential Absorption Lidar (DIAL) instrument [*Browell et al.*, 1990, 1998] observes ozone above and below the aircraft, while the Airborne Raman Ozone, Temperature and Aerosol LIDAR (AROTAL) looks only upwards [*McGee et al.*, 1993, and references therein]. The AROTAL and DIAL observations during PAVE were focused on validation of stratospheric ozone, and are discussed in *Froidevaux et al.* [2007]. This paper

370 considers the DIAL measurements of O_3 during INTEX-B.

371 The DIAL lidar data also include in situ observations from the FASTOZ instrument
372 [*Pearson and Steadman*, 1980; *Eastman and Steadman*, 1977] and interpolation to fill in
373 data for the regions immediately above and below the aircraft, where the LIDAR provides
374 no information. For those portions of the INTEX-B flights that were along the MLS track,
375 the DC-8 was generally flying around 200 hPa. Accordingly, the FASTOZ data contributes
376 significantly to combined LIDAR / in-situ dataset used in these comparisons.

377 In making these comparisons, it is important to bear in mind that MLS data do not
378 represent 'layer means', rather they define piecewise-linear profiles in pressure that best match
379 the observed radiances [*Read et al.*, 2006]. This piecewise linear representation also applies
380 in the along-track direction. Accordingly, the most appropriate manner in which to compare
381 MLS data to high resolution LIDAR measurements is to perform a least-squares fit of the
382 LIDAR data onto the MLS 'grid points' [*Livesey et al.*, 2006]. We have applied such a fit to
383 all the combined DIAL/FASTOZ observations coincident with MLS measurements, (care was
384 taken to avoid situations where the fit effectively resulted in extrapolation).

385 Figure 14 shows a comparison of MLS observations with the results of this fit for all the
386 INTEX-B DIAL coincidences (corresponding flight tracks are shown in right hand column of
387 Figure 20). Good agreement is seen for the high values at 215 hPa, mainly corresponding to
388 stratospheric observations from the 7 May, 2006 flight. The agreement of the few useful points
389 at 147 hPa is somewhat encouraging but far from definitive. The strong vertical gradient in O_3
390 in this region, in combination with proximity to the upper altitude limit of the DIAL data, can
391 lead to additional ambiguities associated with the extrapolation introduced by the least-squares

392 fitting. The large scatter generally seen in these comparisons compared to the MLS error
393 bars may reflect atmospheric variability seen by MLS but not captured by the aircraft. This
394 includes variations across the MLS line of sight (i.e., perpendicular to the DC-8 flight track)
395 and unsampled variability at the altitudes where the DC-8 data represents in interpolation
396 between the DIAL lidar and the FASTOZ in-situ measurements.

Figure 14.

397 **4.2. Comparisons with in-situ aircraft data**

398 **4.2.1. WB-57 Ozone comparisons**

Figure 15.

399 The WB-57 flights during the various AVE campaigns provided several opportunities for
400 comparisons of MLS UT/LS O_3 and CO with in situ observations. While the least-squares
401 fit approach used to map LIDAR observations to the MLS grid is applicable to in situ
402 observations, such fits are very unstable, because of the sparse nature of the aircraft
403 observations. Instead, for all in situ comparisons considered here, we simply compare the
404 MLS data to the average (in mixing ratio space) of all the in situ data points that fall within
405 a 6/decade vertical, 1.5°great circle angle "box" centered on the MLS point. Points where
406 the aircraft departed from the MLS measurement track by more than 100 km or 24 hours
407 were discarded. A summary of all the comparisons of MLS with NOAA O_3 WB-57 data is
408 shown in Figure 15, along with summary statistics for each altitude. Flight tracks for all these
409 comparisons are given in Figure 18.

410 In addition to the usual linear fitting metrics (correlation coefficient, gradient and
411 intercept) we have also computed χ^2 statistics for each of these comparisons. These factor
412 in the uncertainty on both the MLS and aircraft data in quantifying 'goodness of fit'. The

413 'uncertainty' ascribed to the aircraft data (x-axis error bars in the figures) arises not from the
414 raw data themselves, but from trying to compare collections of point measurements to the
415 average over the $\sim 500 \times 4 \times 6$ km volume observed by MLS. The extent to which the multiple
416 aircraft observations within a "box" are representative of the average mixing ratio in that box
417 is hard to quantify, as the amount of atmospheric variability within the box is not completely
418 captured. Simply considering the standard deviation of the in situ data within each box would
419 lend undue weight to those cases where the aircraft sampled only a small fraction of the
420 box. Instead, we have approximated an uncertainty due to this effect as the largest standard
421 deviation (i.e., variability) seen by the aircraft within any of the boxes at a given pressure level
422 for a given flight. For each fit, we show the χ^2 statistics, normalized by the number of degrees
423 of freedom, such that values around unity indicate good fits while larger numbers indicate
424 poor agreement.

425 **4.2.2. WB-57 and DC-8 CO comparisons**

426 The WB-57 payload also included the Argus and 'Aircraft Laser Infrared Absorption
427 Spectrometer' (ALIAS) [*Webster et al.*, 1994] instruments, which provided CO observations.
428 The PAVE and INTEX-B DC-8 missions included CO observations from the Differential
429 Absorption CO Measurements (DACOM) instrument. Figures 16, 17 and 19 summarize these
430 in the same manner as Figure 15, with flight tracks shown in Figures 18 and 20.

431 Unlike for O_3, the observed variability in UT/LS CO is small compared to the ~ 20 ppbv
432 precision on individual MLS data points. This makes it hard to draw definitive conclusions
433 from the in situ comparisons. Many of the Argus and ALIAS comparisons at 147 hPa lie

Figure 16.
Figure 17.
Figure 18.
Figure 19.
Figure 20.

within 1-σ of the one-to-one line, with the majority within 2-σ. The largest differences (50 – 100 ppbv) are seen in the 215 hPa comparisons. At these altitudes, MLS also consistently reports values ∼50–100 ppbv higher than are seen by DACOM. All the comparisons at 215 hPa (notably those with DACOM) show results consistent with the comparisons shown earlier (e.g., with MOZAIC) indicating a factor of ∼2 high bias in the MLS observations. There is a notable lack of correlation between MLS and DACOM for the 31 January 2005 PAVE and 1 May 2006 INTEX-B DC-8 flights. We note, however, that neither flight was targeting MLS validation and the coincidences are poorer than for other comparisons.

Drawing more quantitative conclusions is challenging. In all cases, χ^2 statistics imply no significant departs from a 1-1 relationship for the MLS data at 147 hPa or lesser pressures. Highly significant departures from a 1-1 relationship are indicated for all the 215 hPa MLS v2.2 CO comparisons, but no significant departures are seen from the individual linear fits. These comparisons highlight the difficulties associated with comparing measurements with disparate precisions and vastly different sampling volumes using only a few data points.

5. Summary, conclusions and future plans

Version 2.2 of the MLS data processing algorithms produce O_3 and CO profiles that are scientifically useful in the upper troposphere / lower stratosphere at pressures of 215 hPa and smaller. However, in the case of the 215 hPa CO product, the observed factor of ∼2 high bias compared to other observations needs to be borne in mind, and studies generally limited to considerations of morphology only. The vertical resolution for the O_3 product is ∼2.5 km, with ∼4 km for CO. The cross-track horizontal resolution for both products is ∼6 km and

along-track is ∼100–350 km for O_3, and ∼500–600 km for CO. Individual profiles (spaced ∼165 km along the MLS track) have a typical precision in the UT/LS of 20 – 40 ppbv for O_3 and 15 – 40 ppbv for CO. When using MLS data in scientific studies, care must be taken to screen the data according to the rules given in Section 2.2 [*Livesey et al.*, 2007].

The expected resolution, precision and accuracy of the MLS v2.2 O_3 and CO data are summarized in Table 1. The accuracy to be used in scientific studies is given by the bias uncertainty plus the value times the scaling uncertainty. The overall error bar to use for a point is this accuracy plus the precision as scaled according to the number of points that go into a given average.

Comparisons with expectations and other observations generally corroborate the scientific usefulness of these products. The O_3 data show good agreement with expectations and observations, broadly in line with the systematic error study above. The most notable anomaly is the significant (factor of ∼2) high bias in the MLS CO product at 215 hPa. This is inconsistent with the systematic error budget described in Section 2.5 that estimated a possible ±40 ppbv, ±30% bias. This clearly indicates limitations in our error quantification. This disconnect may lie in the assumptions of linearity used in the quantification of some of the smaller error sources. The MLS radiance signatures in the upper troposphere generally exhibit non-linear dependence on the atmospheric state. This issue will be the focus of future study.

The comparisons described here show no evidence for a bias in the MLS v2.2 O_3 at 215 hPa larger than ∼15%. However, we note that comparisons with SAGE [*Froidevaux et al.*, 2007] and radiosondes [*Jiang et al.*, 2007] indicate a ∼20% high bias in MLS v2.2 O_3 at 215 hPa at mid and high latitudes, although comparisons with ground based LIDAR [*Jiang*

477 *et al.*, 2007] show good agreement in this region. Given these disagreements we ascribe an
478 accuracy of ± 20 ppbv and $\pm 20\%$ to the v2.2 MLS 215 hPa O_3.

479 The bias in the v2.2 MLS upper tropospheric CO data compared to other observations
480 clearly needs further investigation. Further studies are needed to ascertain the nature of this
481 bias (absolute offset, scaling error etc.). More detailed comparisons with MOZAIC and other
482 satellite observations will yield more insight here. Understanding the origin of the CO bias
483 and hopefully correcting it is an important goal for future versions of the MLS data processing
484 algorithms. Planned research will also seek to extend the useful range of these data lower in
485 the troposphere, and further reduce the sensitivity to contamination by thick clouds.

Table 1.

486 **Acknowledgments.** The research described in this paper was carried out by the Jet Propulsion
487 Laboratory, California Institute of Technology, under a contract with the National Aeronautics
488 and Space Administration. We are very grateful to the MLS instrument and data operations and
489 development team for their support through all the phases of the MLS project, in particular D. Flower,
490 G. Lau, J. Holden, R. Lay, M. Loo, D. Miller, B. Mills, S. Neely, G. Melgar, A. Hanzel, M. Echeverri,
491 A. Mousessian and C. Vuu. We greatly appreciate the efforts of B. Bojkov and the Aura Validation
492 Data Center (AVDC) team, whose work facilitated the MLS validation activities. Many thanks are due
493 to the Aura Project for their support throughout the years (before and after Aura launch), in particular
494 M. Schoeberl, A. Douglass (also as co-chair of the Aura validation working group), E. Hilsenrath,
495 and J. Joiner. We also acknowledge the support from NASA Headquarters, P. DeCola for MLS and
496 Aura, and M. Kurylo, J. Gleason, B. Doddridge, and H. Maring, especially in relation to the Aura
497 validation activities and campaign planning efforts. The aircraft campaigns themselves involved tireless

hours from various coordinators, including D. Fahey, E. Jensen, P. Newman, M. Schoeberl, H. Singh, D. Jacob as well as K. Thompson, and others involved with campaign flight management and support. The authors thank D. Edwards and L. Emmons for useful discussions. The authors acknowledge, for their strong support, the European Commission, Airbus the Airlines (Lufthansa, Austrian and Air France), CNRS, Météo-France and Forschungszentrum Jülich who, since 1994, have maintained and carried, free of charge the MOZAIC equipment. MOZAIC is supported by the “Institute National des Sciences de l’Univers – Centre National de la Recherce Scientifique”, France, “Météo France” and “Forshungszentrum Jülich”, Germany. We thank the reviewers and the editor for helpful comments and suggestions to improve this paper.

References

Bey, I., et al. (2001), Global modeling of tropospheric chemistry with assimilated meteorology: Model description and evaluation, *J. Geophys. Res.*, *106*, 23,073–23,096.

Browell, E. V., S. Ismail, and W. B. Grant (1998), Differential absorption lidar (DIAL) measurements from air and space, *Appl. Phys. B*, *67*, 399–410.

Browell, E. V., et al. (1990), Airborne lidar observations in the wintertime Arctic stratosphere: Ozone, *Geophys. Res. Lett.*, *17*, 325–328.

Eastman, J. A., and D. H. Steadman (1977), A fast response sensor for ozone eddy-correlation flux measurements, *Atmos. Environ.*, *11*, 1209–1211.

Filipiak, M. J., et al. (2005), Carbon monoxide measured by the EOS Microwave Limb Sounder on Aura: First results, *Geophys. Res. Lett.*, *32*(14), L14,825, doi:1029/2005GL022765.

Folkins, I., P. Bernath, C. Boone, G. Lesins, N. Livesey, A. M. Thompson, K. Walker, and J. C. Witte (2006), Seasonal cycles of O_3, CO, and convective outflow at the tropical tropopause, *Geophys. Res. Lett.*, *33*, L16,802, doi:10.1029/2006GL026602.

Froidevaux, L., et al. (2006), Early validation analyses of atmospheric profiles from EOS MLS on the Aura satellite, *IEEE Trans. Geosci. Remote Sens.*, *44*(5), 1106–1121.

Froidevaux, L., et al. (2007), Validation of EOS Microwave Limb Sounder stratospheric and mesospheric O_3 measurements, *J. Geophys. Res.*, submitted.

Fu, R., et al. (2005), Short circuit of water vapor and polluted air to the global stratosphere by convective transport over the Tibetan Plateau, *Proc. Nat. Acad. Sci.*, *103*(5664–5669).

527 Intergovernmental Panel on Climate Change (2001), *Climate Change 2001, The Scientific*
528 *Basis*, Cambridge University Press.

529 Jacob, D. J. (1999), *Introduction to Atmospheric Chemistry*, Princeton.

530 Jiang, Y., et al. (2007), Validation of the Aura Microwave Limb Sounder ozone by ozonesonde
531 and lidar measurements, *J. Geophys. Res.*, in review.

532 Li, Q. B., et al. (2005), Convective outflow of South Asian pollution: A global CTM
533 simulation compared with EOS MLS observations, *Geophys. Res. Lett.*, *32*(14),
534 L14,826, doi:10.1029/2005GL022762.

535 Liu, H., D. J. Jacob, I. Bey, R. M. Yantosca, B. N. Duncan, and G. W. Sachse (2003), Transport
536 pathways for Asian pollution outflow over the Pacific: Interannual and seasonal
537 variations, *J. Geophys. Res.*, *108*(D20), 8786, doi:10.1029/2002JD003102.

538 Livesey, N. J., and W. G. Read (2000), Direct retrieval of line-of-sight atmospheric structure
539 from limb sounding observations, *Geophys. Res. Lett.*, *27*(6), 891–894.

540 Livesey, N. J., W. V. Snyder, W. G. Read, and P. A. Wagner (2006), Retrieval algorithms for
541 the EOS Microwave Limb Sounder (MLS), *IEEE Trans. Geosci. Remote Sens.*, *44*(5),
542 1144–1155.

543 Livesey, N. J., et al. (2005), EOS MLS version 1.5 Level 2 data quality and description
544 document, *Tech. rep.*, Jet Propulsion Laboratory (Internal Report), D-32381.

545 Livesey, N. J., et al. (2007), EOS MLS version 2.2 Level 2 data quality and description
546 document, *Tech. rep.*, Jet Propulsion Laboratory (Internal Report).

547 Marenco, A., et al. (1998), Measurement of ozone and water vapor by Airbus in-service
548 aircraft: The MOZAIC airborne program, an overview, *J. Geophys. Res.*, *103*(D19),
549 25,631–25,642.

550 McGee, T. J., M. Gross, R. Ferrare, W. S. Heaps, and U. Singh (1993), Raman DIAL
551 measurements of stratospheric zone in the presence of volcanic aerosols, *Geophys.*
552 *Res. Lett.*, *20*, 955–958.

553 Nedelec, P., V. Thouret, J. Brioude, B. Sauvage, J.-P. Cammas, and A. Stohl (2005), Extreme
554 CO concentrations in the upper troposphere over northeast Asia in June 2003 deom the
555 in situ MOZAIC aircraft data, *Geophys. Res. Lett.*, *32*, L14,807.

556 Nédélec, P., et al. (2003), An improved infra-red carbon monoxide analyser for routine
557 measurements aboard commercial Airbus aircraft: Technical validation and first
558 scientific results of the MOZAIC III program, *Atmos. Chem. Phys.*, pp. 1551–1564.

559 Pearson, R. W., and D. H. Steadman (1980), Instrumentation for fast response ozone
560 measurements from aircraft, *Atmos. Tech.*, *12*.

561 Prather, M. J., and D. J. Jacob (1997), A persistent imbalance in HO_x and NO_x photochemistry
562 of the upper troposphere driven by deep tropical convection, *Geophys. Res. Lett.*,
563 *24*(24), 3189–3192.

564 Pumphrey, H. C., et al. (2007), Validation of middle-atmosphere carbon monoxide retrievals
565 from MLS on Aura, *Journal of Geophysical Research*, (Submitted).

566 Read, W. G., Z. Shippony, M. J. Schwartz, N. J. Livesey, and W. V. Snyder (2006), The

clear-sky unpolarized forward model for the EOS Microwave Limb Sounder (MLS), *IEEE Trans. Geosci. Remote Sens.*, *44*(5), 1367–1379.

Read, W. G., et al. (2007), EOS Aura Microwave Limb Sounder upper tropospheric and lower stratospheric humidity validation, *J. Geophys. Res.*, (Submitted).

Rodgers, C. D. (2000), *Inverse Methods for Atmospheric Science, Theory and Practice*, 238 pp., World Scientific.

Santee, M. L., et al. (2007), Validation of Aura Microwave Limb Sounder nitric acid measurements, *This issue*.

Schoeberl, M. R., B. N. Duncan, A. R. Douglass, J. W. Waters, N. J. Livesey, W. G. Read, and M. J. Filipiak (2006a), The carbon monoxide tape recorder, *Geophys. Res. Lett.*, *33*, L12,811, doi: 10.1029/2006GL026178.

Schoeberl, M. R., et al. (2006b), Overview of the EOS Aura mission, *IEEE Trans. Geosci. Remote Sens.*, *44*(5), 1066–1074.

Stohl, A., S. Eckhardt, C. Forster, P. James, and N. Spichtinger (2002), On the pathways and timescales of intercontinental air pollution transport, *J. Geophys. Res.*, *107*(D23), 4684, doi:10.1029/2001JD001396.

Thouret, V., A. Marenco, J. A. Logan, P. Nédélec, and C. Grouhel (1998), Comparison of ozone measurements from the MOZAIC airborne programand the ozone sounding network at eight locations, *J. Geophys. Res.*, *103*, 25,695–25,720.

586 Waters, J. W., et al. (2006), The Earth Observing System Microwave Limb Sounder (EOS
587 MLS) on the Aura satellite, *IEEE Trans. Geosci. Remote Sens.*, *44*(5), 1075–1092.

588 Webster, C. R., R. D. May, C. A. Trimble, R. G. Chave, and J. Kendall (1994), Aircraft
589 (ER-2) Laser Infrared Absorption Spectrometer (ALIAS) for in situ stratospehric
590 measurements of HCl, H_2O, CH_4, NO_2, and HNO_3, *Appl. Optics*, *33*, 454–472.

591 Received _____

592 This manuscript was prepared with AGU's LaTeX macros v5, with the extension package
593 'AGU^{++}' by P. W. Daly, version 1.6b from 1999/08/19.

Figure Captions

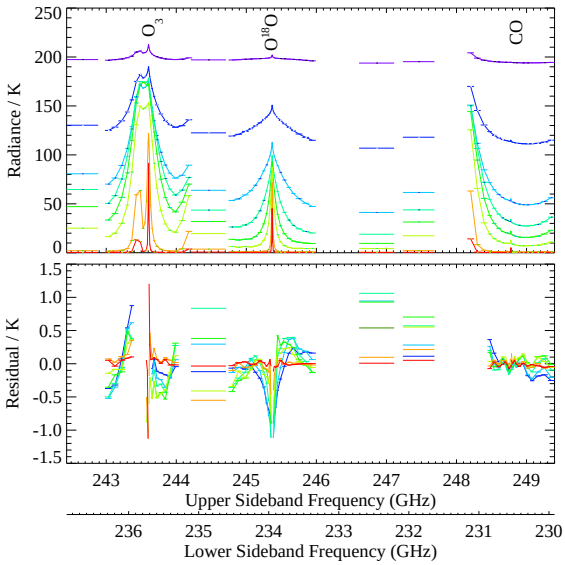

Figure 1. (Top) sample radiances (shown in terms of brightness temperature) from the MLS 240 GHz radiometer. Global average radiances from observations on 24 September 2004 are shown for 8 selected tangent point altitudes ranging from ~7.5 km (purple) to ~45 km (red). The MLS signal is a combination of incoming radiance at frequencies above (upper sideband, upper x-axis) and below (lower sideband, lower x-axis) the 239.660 GHz local oscillator. The widths of the various MLS spectral channels are denoted by the horizontal bars. The position of O_3, $O^{18}O$ and CO emission lines are noted. (Bottom) The average fit achieved to these radiances by the MLS version 2.2 retrieval algorithms. Some channels are not used in the retrievals, and so are not in the lower panel (e.g., those around 243.5 GHz upper sideband frequency).

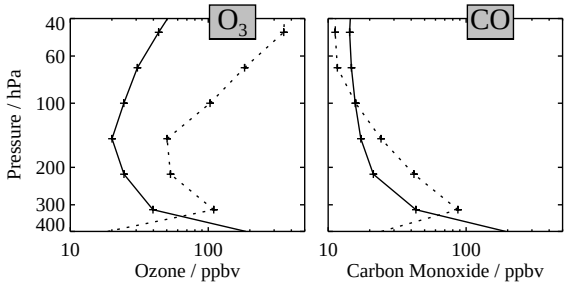

Figure 2. Root-mean-square estimated precision (solid line) and 1-σ scatter (dashed line) seen in the MLS UT/LS O_3 (left) and CO (right) measurements on 17 September 2004 in the 30°S – 30°N region.

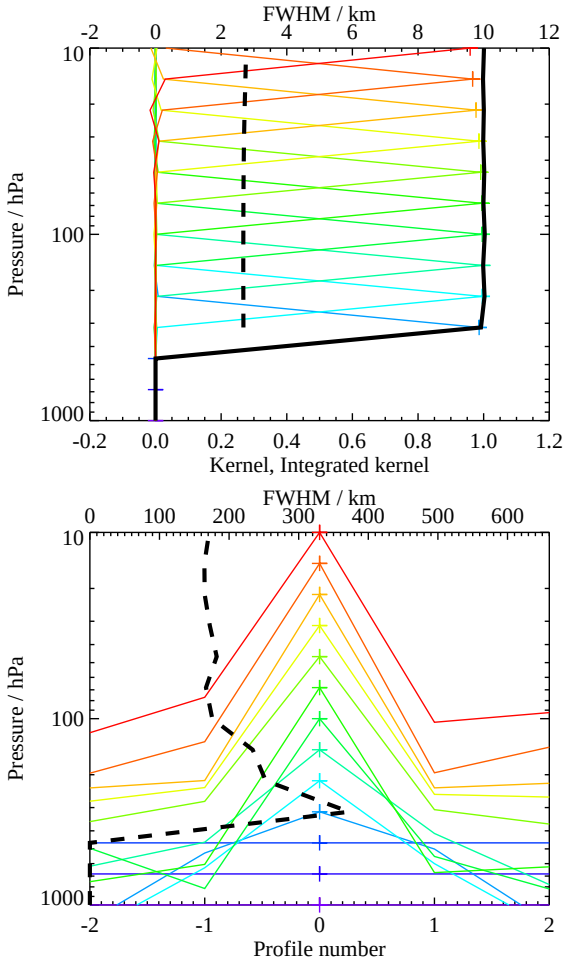

Figure 3. Two-dimensional (vertical and horizontal along-track) averaging kernels for the MLS v2.2 O_3 data at the equator. Colored lines for each retrieval level (denoted by the plus signs) show the averaging kernels. The dashed black lines indicate the resolution, determined from the full width at half maximum (FWHM) of the averaging kernels, approximately scaled into kilometers (top axes). (Top) Vertical averaging kernels (lower axis, integrated in the horizontal dimension for five along-track profiles) and resolution. The solid black line shows the total integrated area under each kernel (lower axis); (Bottom) Horizontal averaging kernels (integrated in the vertical dimension). The individual horizontal averaging kernels, shown as a function of retrieved profile (lower axis), are scaled in the y-axis direction such that a unit change is equivalent to one decade in pressure.

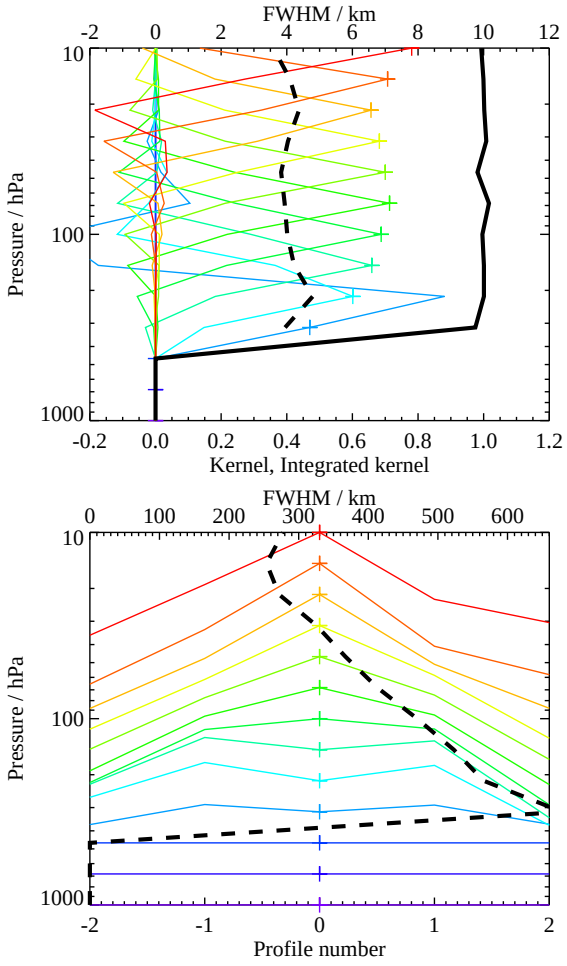

Figure 4. As Figure 3 but for MLS v2.2 CO.

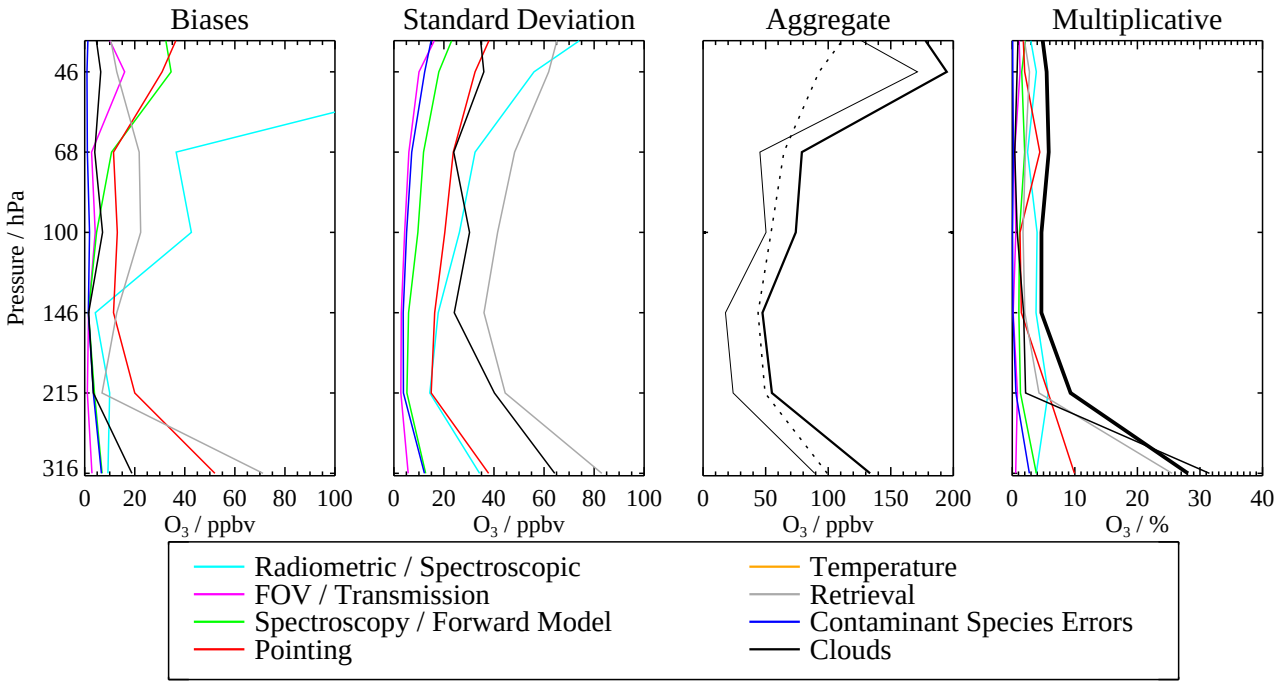

Figure 5. The estimated impact of various systematic error families on the MLS UTLS O_3 observations. The first two panels show the (first) possible biases, and (second) standard deviation of the additional scatter, introduced by the various families of errors. Colored lines denote the contributions due to uncertainties in: MLS radiometric and spectral calibration (cyan), field of view and antenna transmission efficiency (magenta) pointing (red), spectroscopic databases and forward model approximations (green), temperature retrievals (gold), other MLS products (blue). Errors due to retrieval approximations are shown in grey, and the typical impact of cloud contamination is denoted by the black line. (Third panel) the root sum squares (RSS) of all the possible biases (thin solid line), all the additional scatters (thin broken line), and the RSS sum of the two (thick solid line). (Fourth panel) the scaling uncertainties introduced by the various error sources (colors have the same meaning as for the first two panels). The thick black line shows the RSS scaling uncertainty.

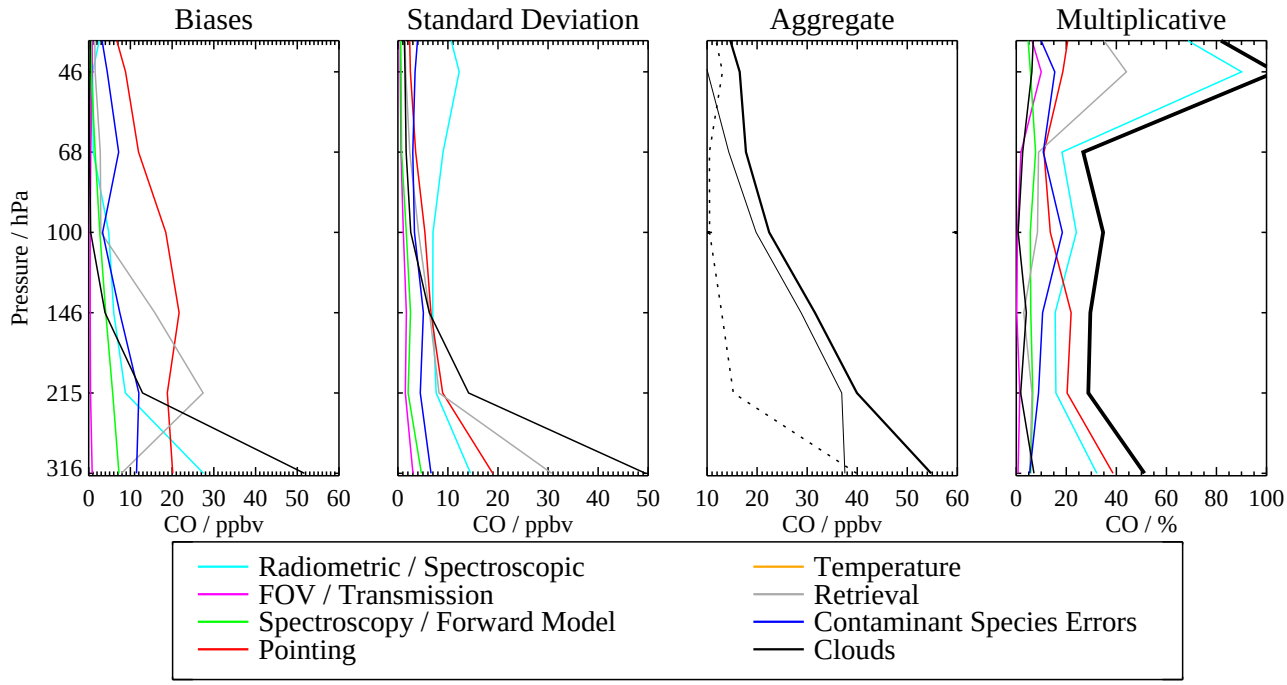

Figure 6. As Figure 5 except for UT/LS CO.

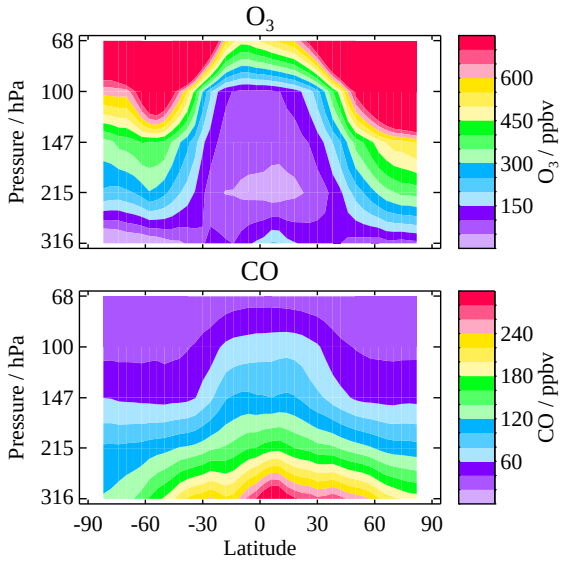

Figure 7. Zonal means from ~80 days (distributed across seasons and years) of MLS v2.2 O_3 and CO data in the UT/LS region.

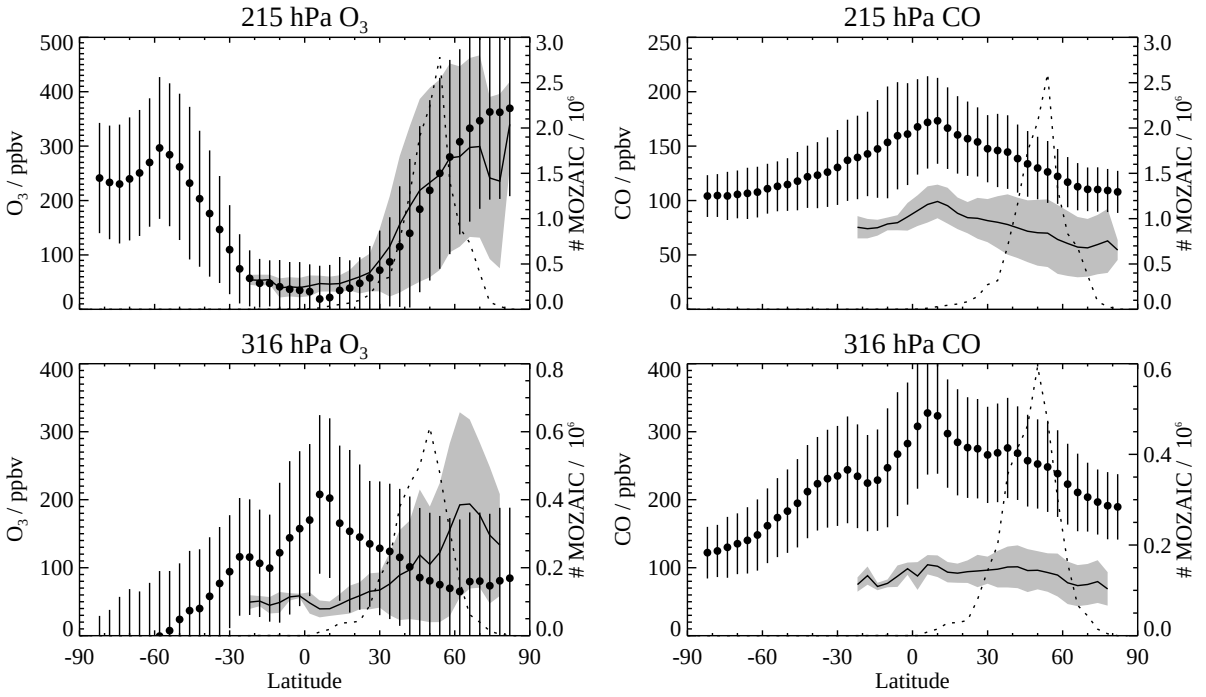

Figure 8. Zonal means (left hand axes) of MOZAIC (left panels) O_3 and (right panels) CO data for 2004 and 2005 (solid line plus grey shading indicating standard deviation), compared to the MLS zonal means shown in Figure 7 (points, with 'error bars' indicating standard deviation). The broken lines indicate the number of MOZAIC measurements that formed the averages (right hand axes). The '316 hPa' MOZAIC data is an average of all the measurements from 383 –261 hPa, while the '215 hPa' values are the 261 – 177 hPa average. Uncertainties on the MOZAIC observations are 2 ppbv precision, 2% accuracy for O_3, and 5 ppbv precision, 5% accuracy for CO.

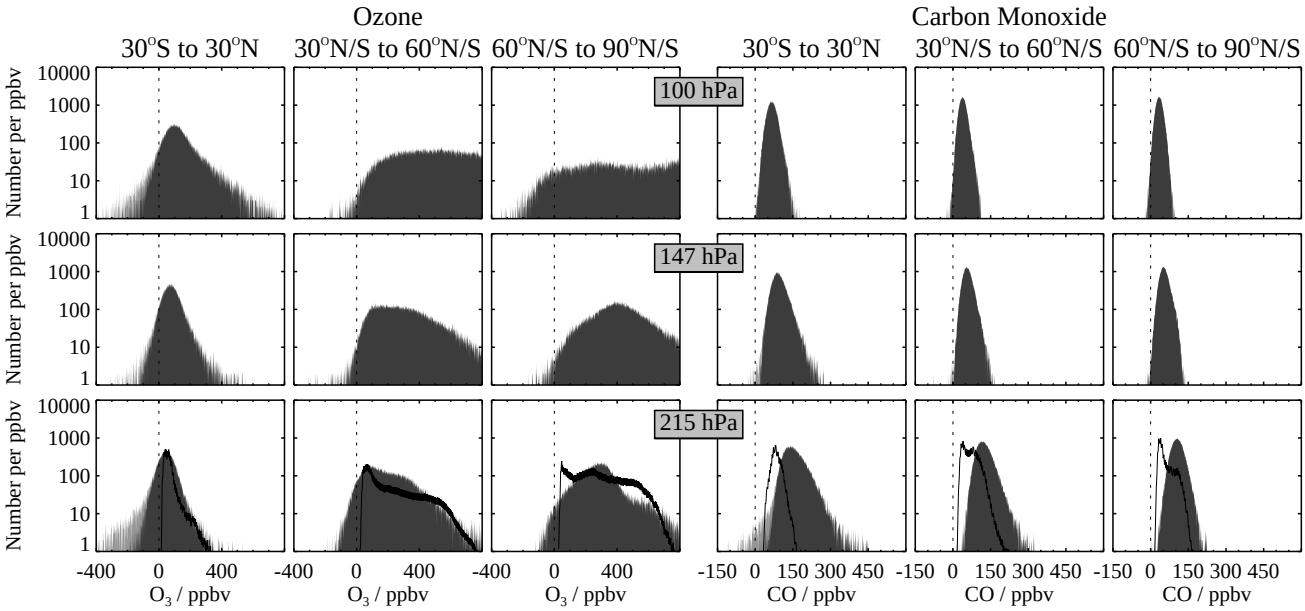

Figure 9. Histograms of all the MLS UT/LS O_3 and CO data for ~80 days (distributed across seasons and years) in three latitude bins (tropics, mid-latitudes and polar regions). The light grey histogram shows all the MLS data for which the 'Status' field is an even number and the precision field is positive. The darker grey region shows those values meeting the 'Quality' and 'Convergence' screening described in section 2.2. The black lines show the comparable histogram for 2004 – 2005 MOZAIC data (renormalized vertically to fit the same scale).

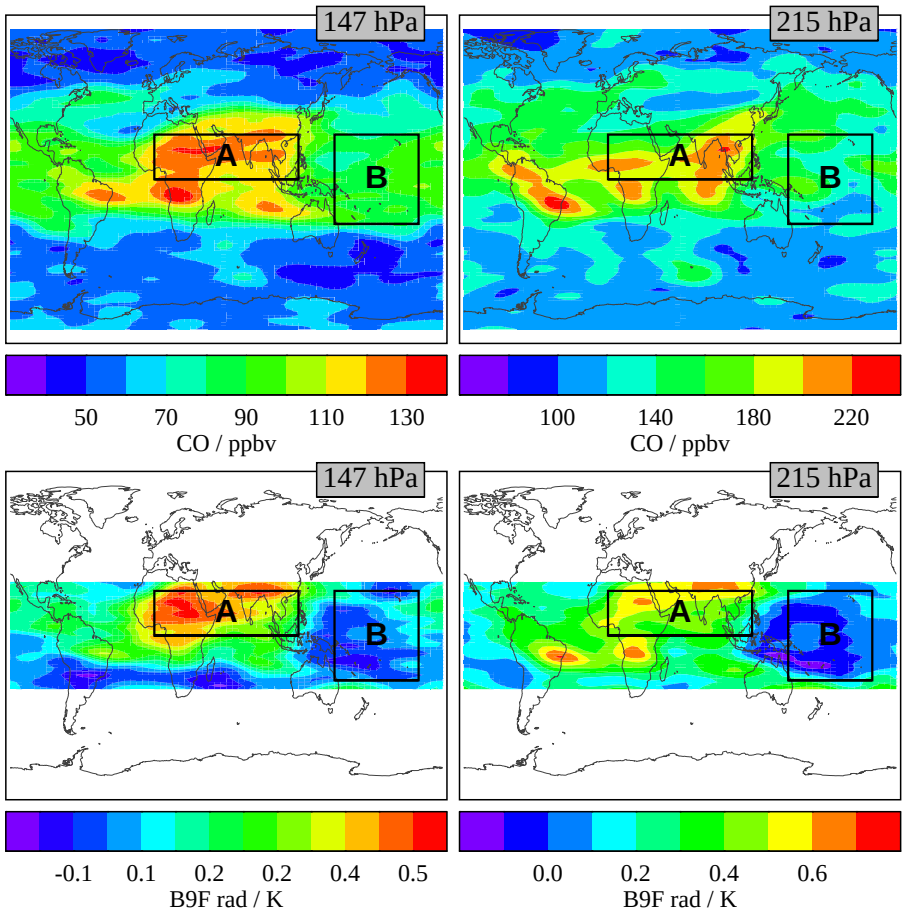

Figure 10. (Top) Maps of average v2.2 MLS CO at 147 hPa and 215 hPa from the period 17 – 19 September 2004. (Bottom) Maps of the CO radiance metric described in the text for the same period.

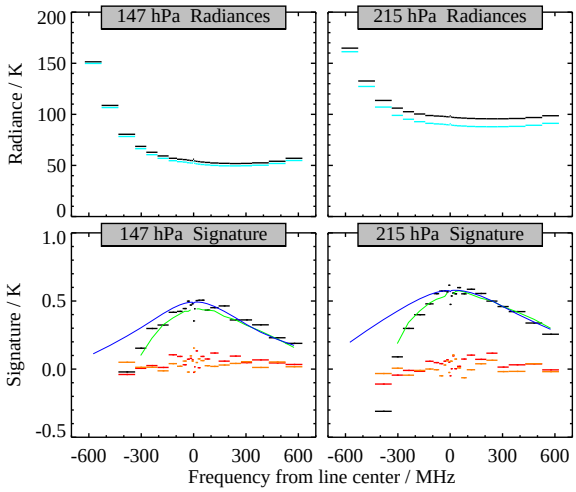

Figure 11. Top: Comparison of average MLS radiances measured in region A of the maps in Figure 10 (black) with those in region B (cyan). Bottom: Black lines show region A minus region B radiance differences when the signatures of continuum emission and upper tropospheric ozone have been removed as described in the text. Green lines show the same difference for the fit to the measured radiances achieved by the v2.2 software. Blue lines show the expected shape of the CO contribution at these altitudes. The orange and red lines show the difference in measured radiances between the northern and southern (red) and eastern and western (orange) halves of region B. In these cases no signature of CO is seen in the differences.

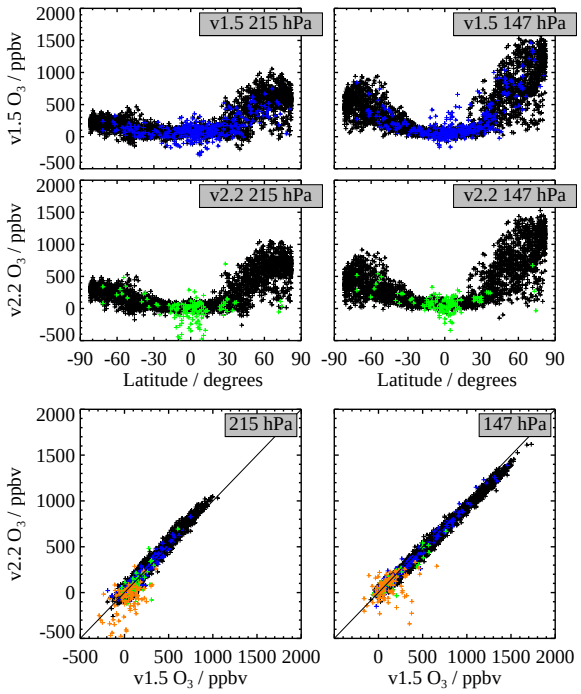

Figure 12. Comparison of MLS v1.5 and v2.2 O_3 data for 1 May 2006. The left hand plots show data at 215 hPa, with 147 hPa data shown on the right. The top row shows MLS v1.5 O_3 data as a function of latitude. Black points meet all the screening criteria given for v1.5 O_3 data (*Livesey et al.* [2005]). Blue points are those v1.5 O_3 points where quality>0.1 or status was a non-zero even number, indicating cloud contamination (points with negative precision or odd values of status are completely neglected in all these plots). The second row of plots shows the equivalent for v2.2 O_3, with the green points being those where quality>1.2 or convergence<1.8 (see Section 2.2, the status=0 criteria is not required for v2.2 data). The final row of plots scatters the v2.2 data (y-axis) against v1.5 (x-axis) with black points indicating data that was 'good' in both datasets, blue and green indicating data marked bad by v1.5 and v2.2, respectively, and orange symbols used for points identified as 'bad' in both versions.

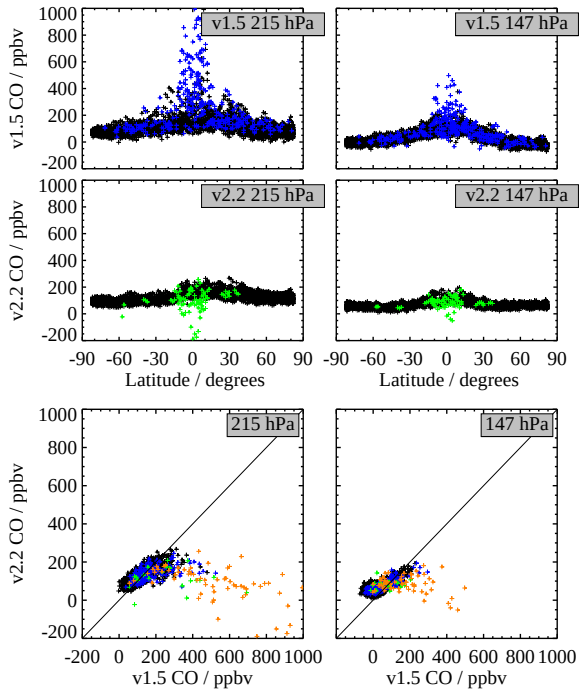

Figure 13. As Figure 12 but for CO. Here the v1.5 screening criterion was Quality>0.05, the v2.2 screening criteria are the same as for O_3.

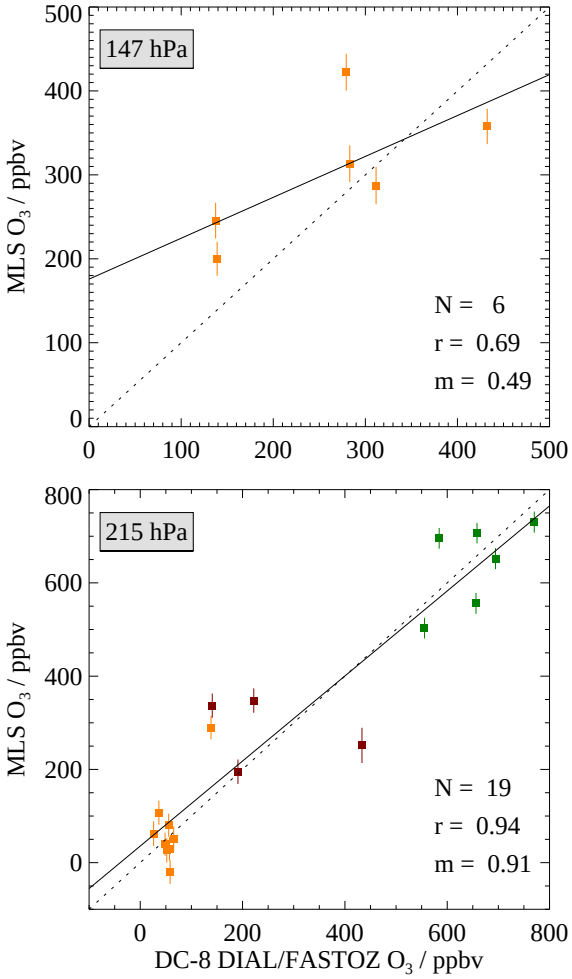

Figure 14. Summary of all the MLS/DIAL LIDAR ozone comparisons. Each data point compares one MLS retrieved O_3 value (y-axis) with an estimate from a least-squares fit to INTEX-B LIDAR data. The error bars denote the MLS precision estimates. Different colors are used to denote different DC-8 flights, see Figure 20 for details. The number of points (N), correlation coefficient (r) and linear fit gradient (m) are quoted for each panel.

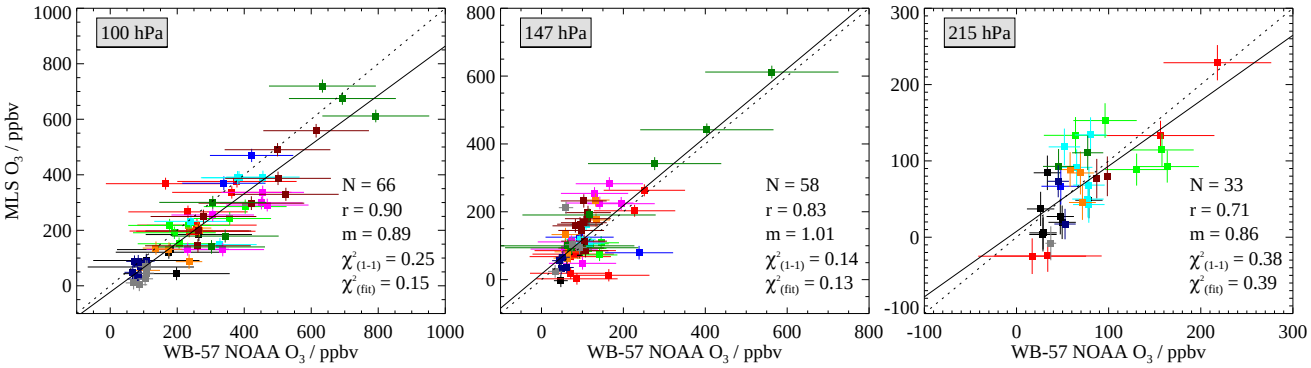

Figure 15. Summary of all MLS/WB-57 O_3 comparisons. Points are individual MLS O_3 values (y-axis) compared to average nearby in situ observations (x-axis). Y-axis error bars show the estimated precision of MLS O_3. X-axis error bars show the variability seen in the WB-57 observations as described in the text. Different colors denote different flights, as shown on Figure 18. The solid line is the least-squares linear fit to the data, and the broken line shows the one-to-one correlation line. The number of points (N), correlation coefficient (r) and linear fit gradient (m) are quoted for each panel. In addition two normalized χ^2 metrics are shown one for a one-to-one correspondence, the other for the linear fit.

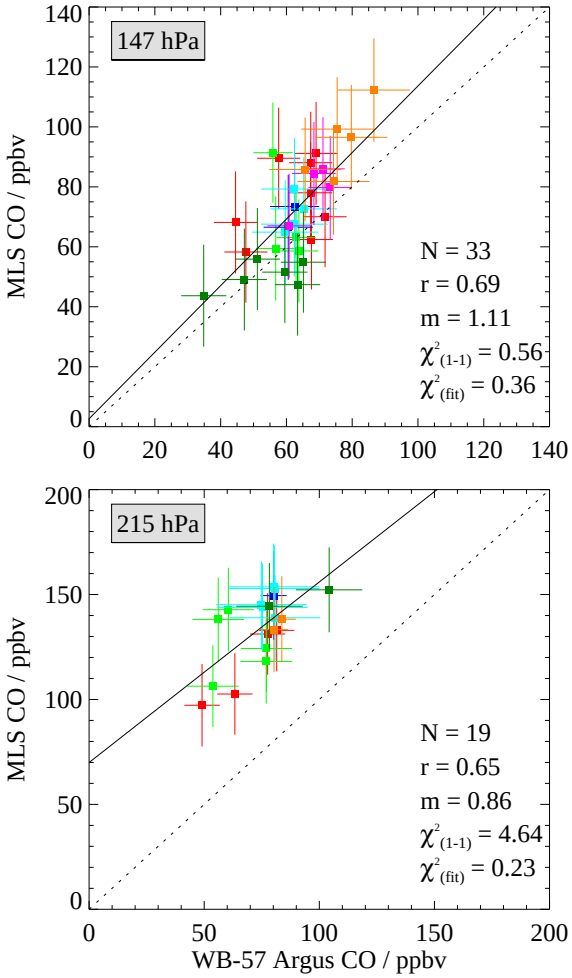

Figure 16. As Figure 15 except comparing MLS CO with WB-57 Argus observations. The estimated absolute accuracy for Argus data is 2%, traceable to CMDL standards.

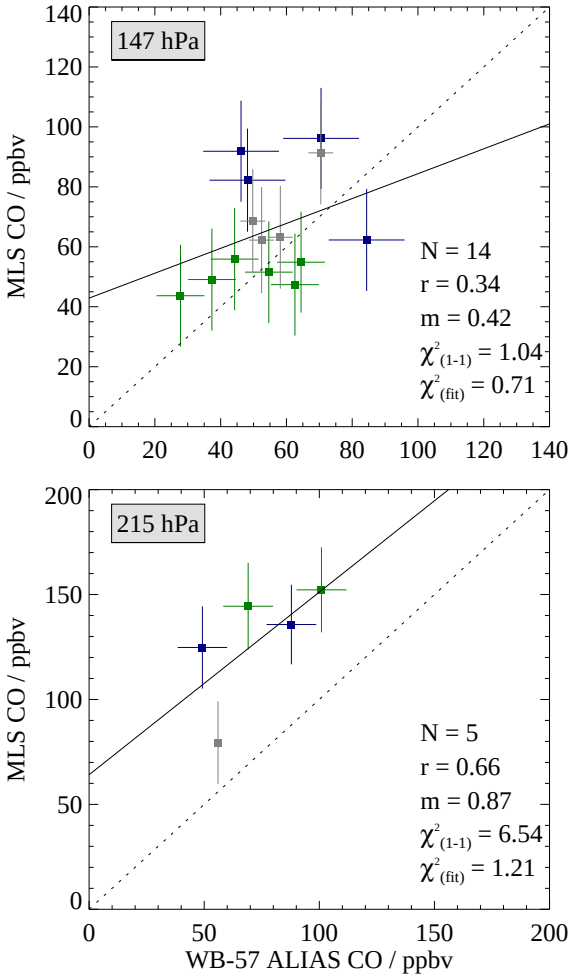

Figure 17. As Figure 15 comparing MLS CO to measurements from WB-57 ALIAS measurements during the Costa-Rica AVE campaign.

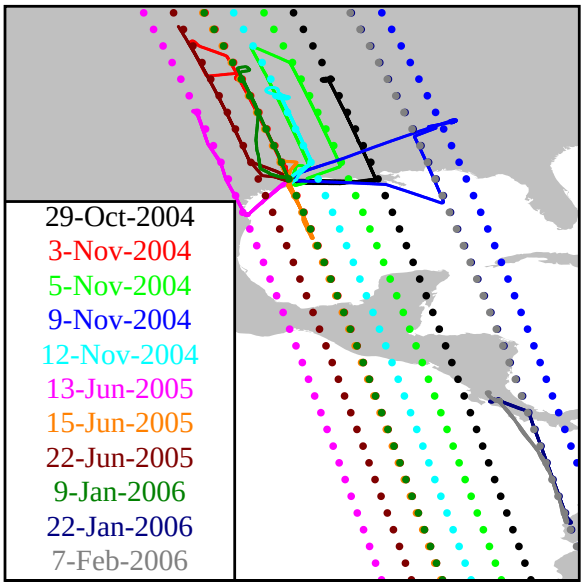

Figure 18. Map showing all the WB-57/MLS coincidences during the AVE missions. Colors are as used in Figures 15, 16 and 17.

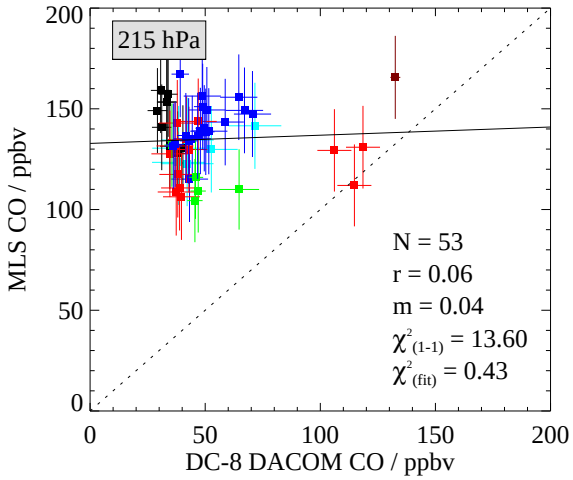

Figure 19. As for Figure 15 except comparing MLS CO to observations from DACOM on the NASA DC-8. The large bias seen here is consistent with the Argus and ALIAS comparisons at 215 hPa indicating a factor of 2 high bias. The colors used for the different flight days are described in Figure 20, except for Magenta which is for a 22 March INTEX-B transfer flight.

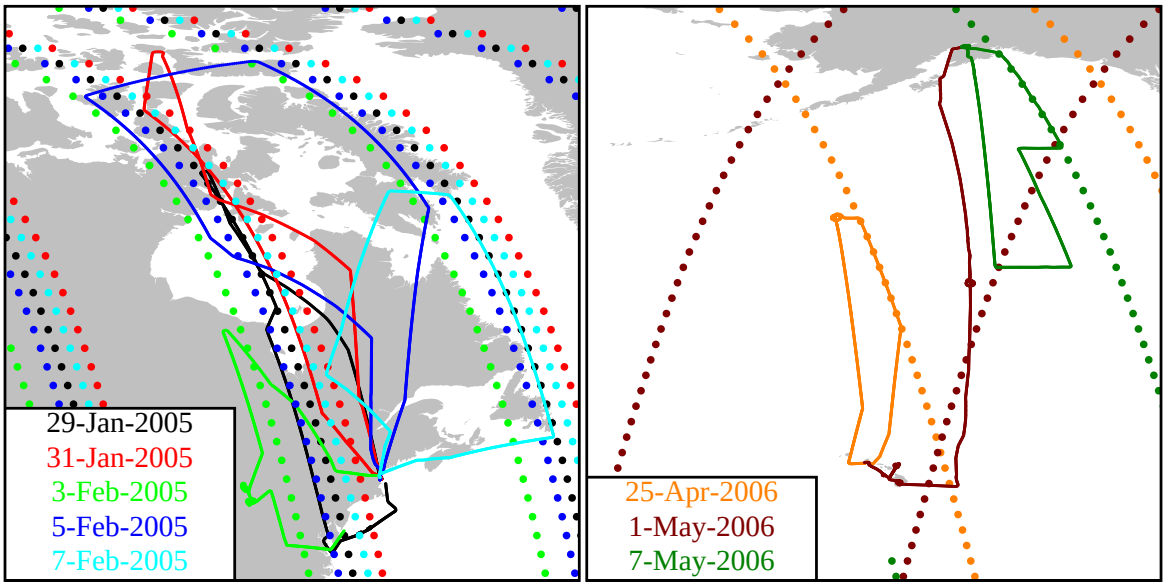

Figure 20. Maps showing the DC-8/MLS coincidences during the PAVE (top) and INTEX-B (lower) missions. Colors are as used in Figures 14 and 19. The 22 March 2006 flight in the INTEX-B campaign which was a transfer from Houston to NASA-AMES is not shown.

Tables

Table 1. Summary of MLS UT/LS O_3 (upper) and CO (lower) products

Pressure	Resolution[a] / km	Precision[b] / ppbv	Bias uncertainty / ppbv	Scaling uncertainty	Comments
			MLS O_3 product		
46 hPa and less	—	—	—	—	See Froidevaux et al. (this issue)
68 hPa	3×200	± 50	± 50	$\pm 5\%$	
100 hPa	3×200	± 40	± 50	$\pm 5\%$	
147 hPa	3×200	± 40	± 20	$\pm 5\%$	
215 hPa	3×200	± 40	± 20	$\pm 20\%$[c]	
316 hPa	—	—	—	—	Unsuitable for scientific use
1000 – 464 hPa	—	—	—	—	Not retrieved
			MLS CO product		
46 hPa and less	—	—	—	—	See Pumphrey et al. (this issue)
68 hPa	4×400	± 10	± 10	$\pm 30\%$	
100 hPa	4×500	± 20	± 20	$\pm 30\%$	
147 hPa	4×500	± 20	± 30	$\pm 30\%$	
215 hPa	5×600	± 20	± 40	$\sim +100\%$ [d]	See text
316 hPa	—	—	—	—	Unsuitable for scientific use
1000 – 464 hPa	—	—	—	—	Not retrieved

[a] Vertical $\times$ along-track. Cross-track resolution is $\sim$6 km

[b] Precision on individual profiles

[c] Indicated by comparisons with other observations described in this and other papers, rather than from the predictions used for other levels, see text for discussion

[d] Indicated by comparisons with other observations, rather than from the predictions used for other levels, see text for discussion